Effect of cohesion on internal stability of bilinear geosynthetic-reinforced slopes

IOP Conf. Series: Materials Science and Engineering **542** (2019) 012011 doi:10.1088/1757-899X/542/1/012011

Effect of cohesion on internal stability of bilinear geosynthetic-reinforced slopes

Gongquan Zhang[1] , Xiaobo Ruan[1], Jun Yan[1] and Dayong Zhu[2]

1 School of Automotive and Transportation Engineering, Hefei University of Technology, Hefei, China
2 School of Civil Engineering, Hefei University of Technology, Hefei, China
E-mail: xiaoboruan@163.com

Abstract. This paper presents a limit equilibrium (LE) approach to analyze the internal stability of the bilinear geosynthetic-reinforced slopes comprised of cohesive reinforced fill. This LE analysis uses a top-down log spiral mechanism to formulate the resultant reinforcement force in the lower tier required for internal design of such reinorced slopes. The presented formulation considers both cohesion and depth of crack, and then the required unfactored reinforcement strength is defined and used for subsequent analysis. Results are presented in the form of stability charts, enabling quick assessment of reinforcement strength required for internal stability. In addition, the effect of cohesion and depth of crack on the critical slip surface is discussed, respectively.

1. Introduction

In this paper, a bilinear geosynthetic-reinforced slop can be defined as a geosynthetic-reinforced slope with zero batter (i.e., vertical) in the upper while another geosynthetic-reinforced slope has a batter greater than zero (non-vertical) in the lower. This reinforced slope can yield the same right-of-way as a single equivalent, yet less steep slope. For analysis of bilinear reinforced slopes, Ruan et al. (2015)[1] conducted a rigorous limit equilibrium (LE) analysis exploring the impact of such reinforced slopes on the maximum reinforcement force required for global stability. Subsequently, considering the effect seismic load, Ruan et al. (2017) [2] extended the formulation in the paper of Ruan et al. (2015) [1].

China has a vast territory, and the soil quality varies greatly. In the absence of high quality filling areas, the one-sided pursuit of filler quality may lead to excessive investment. In engineering practice, Yang et al. (2012) [3] has used the cohesive material as the reinforced fill, but the related engineering experience is still immature. Therefore, the study of the relevant characteristics of reinforced earth structures with cohesive materials is helpful to broaden its scope of application, and achieve the purpose of saving project cost and improving economic benefits. In particular, it is necessary to study the effect of cohesion of internal stability of bilinear geosynthetic-reinforced slopes.

The objective of this study is to formulate the resultant reinforcement force required for internal stability of bilinear geosynthetic-reinforced slopes in the lower tier through extending the methods of Ruan et al. (2015) [1] combined with Vahedifard, et al. (2014) [4]. Presented formulation considers the effect of cohesion and depth of crack. In addition, it is assumed that the foundation soil is competent.

2. Formulation

The outlined analysis assumes log spiral slip surfaces as part of the LE formulation – refer to Figure 1 for notation and convention. In Figure 1, the resisting forces, T_1 and T_2, are the resultant force of all

reinforcement layers for the upper tier and the lower tier, respectively. The driving force, *W*, is the weight of the entire failure mass. The line of action of T_1, D_1, is measured from the bottom of the upper tier while the lines of action of T_2, D_2, is measured from the bottom of the lower tier.

The location of the resultant reinforcement force is not known and must be assumed. For the current design guidelines of Mechanically Stabilized Earth walls [5], for a horizontal and surcharge-free crest subjected to static conditions, the height of the resultant is one third of the height of the wall. With assumed surcharge or seismicity, the elevation of resultant goes up. Therefore, it is reasonable to assume D_1 and D_2, to act at $H_1/3$ and $H_2/2$, respectively.

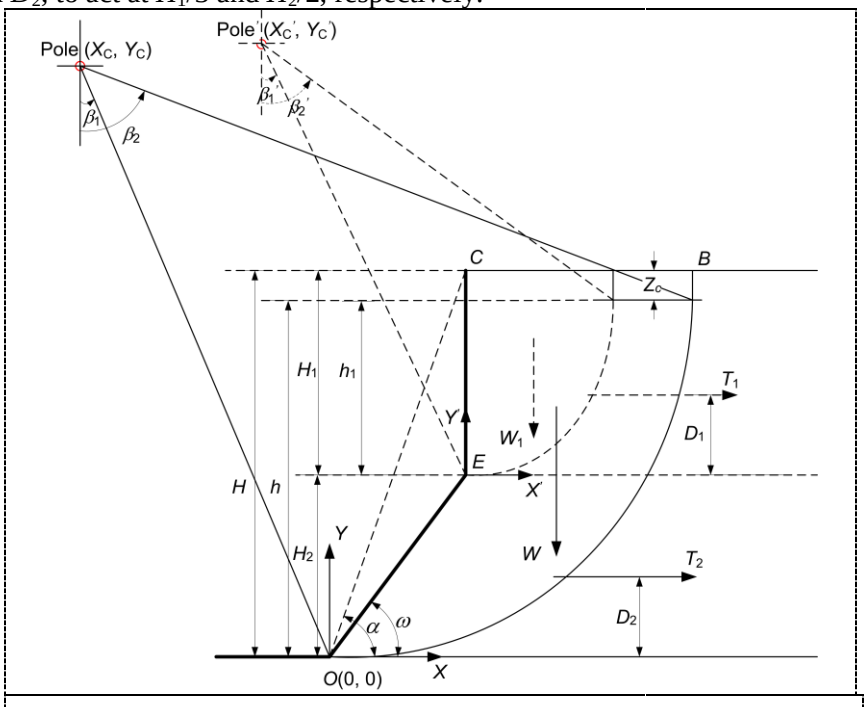

Figure 1. Notation and convention for the presented LE approach..

For completeness, the expression for the resultant resisting force in the upper tier, T_1, is reproduced here from Vahedifard, et al. (2014) [4]

$$
\begin{aligned}
T_1 = \Bigg\{ & \gamma_d \int_{\beta_1'}^{\beta_2'} \left(A' e^{-\psi\beta'} \cos\beta' - A' e^{-\psi\beta_2'} \cos\beta_2' \right) \left(A' e^{-\psi\beta'} \sin\beta' \right) \left(A' e^{-\psi\beta'} \right) \left(\cos\beta' - \psi \sin\beta' \right) d\beta' \\
& - c \int_{\beta_1'}^{\beta_2'} \left(A' e^{-\psi\beta'} \cos\beta' \right) \left(A' e^{-\psi\beta'} \right) \left(\cos\beta' - \psi \sin\beta' \right) d\beta' - c \int_{\beta_1'}^{\beta_2'} \left(A' e^{-\psi\beta'} \sin\beta' \right) \left(A' e^{-\psi\beta'} \right) \\
& \times \left(\sin\beta' + \psi \cos\beta' \right) d\beta' + \frac{1}{2} \gamma_d Z_c \left[\left(A' e^{-\psi\beta_2'} \sin\beta_2' \right)^2 - \left(A' e^{-\psi\beta_1'} \sin\beta_1' \right)^2 \right] \Bigg\} \\
& / \left(A' e^{-\psi\beta_1'} \cos\beta_1' - D_1 \right)
\end{aligned}
\tag{1}
$$

where, γ_d is the unit weight of the reinforced soil; c is the cohesion of reinforced fill; β_1' and β_2' are angles at points where the log spiral slip surface enters and exits the upper tier; β' is the angle in polar coordinates defined relative to Cartesian coordinate system translated to Pole' (X_C', Y_C') from the origin *E* – Fig. 1; A' is log spiral constant, i.e., $h_1 / \left[\exp\left(-\psi\beta_1'\right) \cos\beta_1' - \exp\left(-\psi\beta_2'\right) \cos\beta_2' \right]$, where, h_1=H_1-Z_c, H_1 is height of the upper tier and Z_c is the depth of crack, ψ=tanϕ_d, and ϕ_d is the design internal angle of friction.

The resistive moment component due to normal and shear stress distributions along the log spiral at a LE state vanishes since its elemental resultant force goes through the pole. Consequently, at a LE state the resisting and driving moments are equal as shown:

$$M_W=M_{T1}+M_{T2} \tag{2}$$

where, M_W is the driving moment about the pole and can be calculated using W multiplied by its corresponding leverage arm; M_{T1} and M_{T2} are the resisting moments and can be determined using T_1 and T_2 multiplied by their respective leverage arms, respectively.

Using Eqns. 1 and 2 one can solve T_2 which is as follows

$$\begin{aligned} T_2 = \Big\{ & \gamma_d \int_{\beta_1}^{\beta_2} \left(Ae^{-\psi\beta}\cos\beta - Ae^{-\psi\beta_2}\cos\beta_2\right)\left(Ae^{-\psi\beta}\sin\beta\right)\left(Ae^{-\psi\beta}\right)(\cos\beta-\psi\sin\beta)d\beta \\ & - C\int_{\beta_1}^{\beta_2}\left(Ae^{-\psi\beta}\cos\beta\right)\left(Ae^{-\psi\beta}\right)(\cos\beta-\psi\sin\beta)d\beta - C\int_{\beta_1}^{\beta_2}\left(Ae^{-\psi\beta}\sin\beta\right)\left(Ae^{-\psi\beta}\right) \\ & \times(\sin\beta+\psi\cos\beta)d\beta + \frac{1}{2}\gamma_d Z_c\left[\left(Ae^{-\psi\beta_2}\sin\beta_2\right)^2 - \left(Ae^{-\psi\beta_1}\sin\beta_1+\cot\alpha\right)^2\right] \\ & - \left(\gamma_d h_1 H\cot\alpha\right)\left(Ae^{-\psi\beta_1}\sin\beta_1 + H\cot\alpha/2\right) - \left(\gamma_d H_2 H\cot\alpha/2\right)\left(Ae^{-\psi\beta_1}\sin\beta_1\right. \\ & \left. + H\cot\alpha/3\right) - T_1\left(Ae^{-\psi\beta_1}\cos\beta_1 - H_2 - D_1\right)\Big\} / \left(Ae^{-\psi\beta_1}\cos\beta_1 - D_2\right) \end{aligned} \tag{3}$$

where, H_2 and H are heights of the lower tier and the bilinear slope, respectively; β_1 and β_2 are angles of points where the log spiral enters and exits the bilinear slope – Fig. 1; α is the angle of the bilinear slope; β is the angle in polar coordinates defined relative to Cartesian coordinate system translated to Pole (X_C, Y_C) from the origin O (0, 0); A is log spiral constant, i.e., $h/[\exp(-\psi\beta_1)\cos\beta_1 - \exp(-\psi\beta_2)\cos\beta_2]$, where $h=H-Z_c$.

For a dimensionless analysis using T_1 and T_2, one can respectively define K_{T1} and K_{T2} as $2T_1/(\gamma_d H^2)$ and $2T_2/(\gamma_d H^2)$, respectively

3. Results

3.1. Stability charts

When α=70 °, Z_c=0 and ϕ_d=34 °, Figure 2 shows that K_{T1} increases as λ increases for different values of c while K_{T2} decreases with an increase in λ. In particular, K_{T2} is equal to zero when the value of $c/\gamma_d H$ arrives at 0.075 regardless of the value of λ.

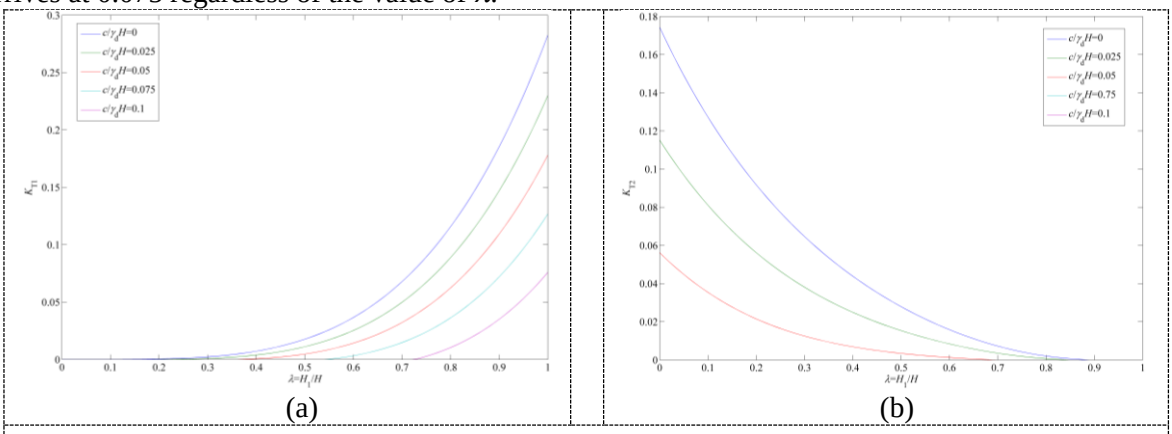

Figure 2. Stability charts for different c and λ when α=70 °: (*a*) K_{T1}, and (*b*) K_{T2}.

When α=80 °, Z_c=0 and ϕ_d=34 °, Figure 3 shows that K_{T1} increases as λ increases for different values of c while K_{T2} decreases with an increase in λ. In particular, K_{T2} is equal to zero when the value of $c/\gamma_d H$ arrives at 0.1 and λ is more than 0.06.

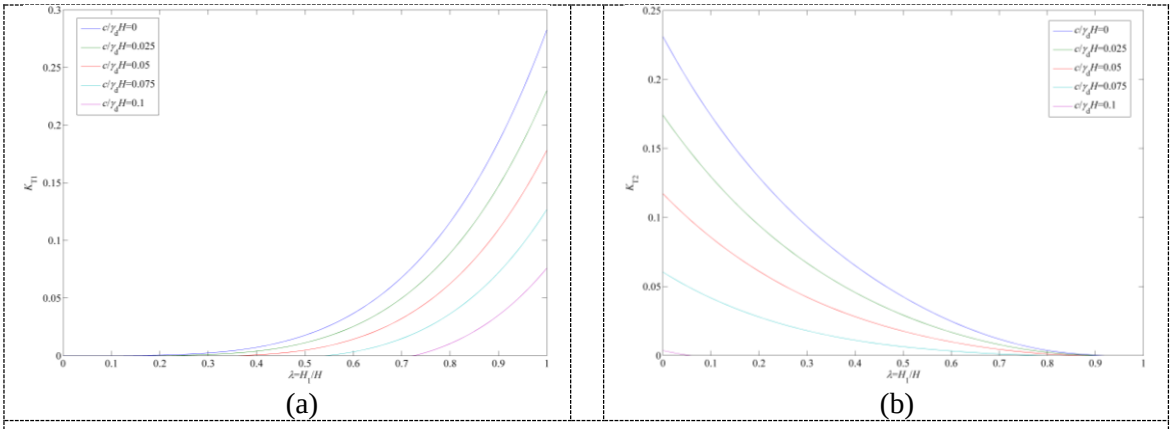

Figure 3. Stability charts for different c and λ when α=80 °: (*a*) K_{T1}, and (*b*) K_{T2}.

3.2. Critical slip surfaces

It is noted that 'critical slip surfaces' means that these surfaces produce maximum T_1 and T_2 forces; hence, they govern design. In Figure 4, traces of critical slip surfaces are presented for different values of c while λ is equal to 0.6, α is equal to 70 °and 80 °, $c/\gamma_d H$ is 0, 0.025, and 0.05, and ϕ_d is equal to 34 °. With the increase of the value of $c/\gamma_d H$, the critical slip surface moves towards the facing in the upper while moves away from the facing in the lower. In Figure 4(*a*), when $c/\gamma_d H$=0, K_{T1}=0.0366, and K_{T2}=0.0158, when $c/\gamma_d H$=0.025, K_{T1}=0.0253, and K_{T2}=0.0248, and when $c/\gamma_d H$=0.05, K_{T1}=0.0142, and K_{T2}=0.0013. In Figure 4(*b*), when $c/\gamma_d H$=0, K_{T1}=0.0366, and K_{T2}=0.0158, when $c/\gamma_d H$=0.025, K_{T1}=0.0253, and K_{T2}=0.0168, and when $c/\gamma_d H$=0.05, K_{T1}=0.0142, and K_{T2}=0.0099.

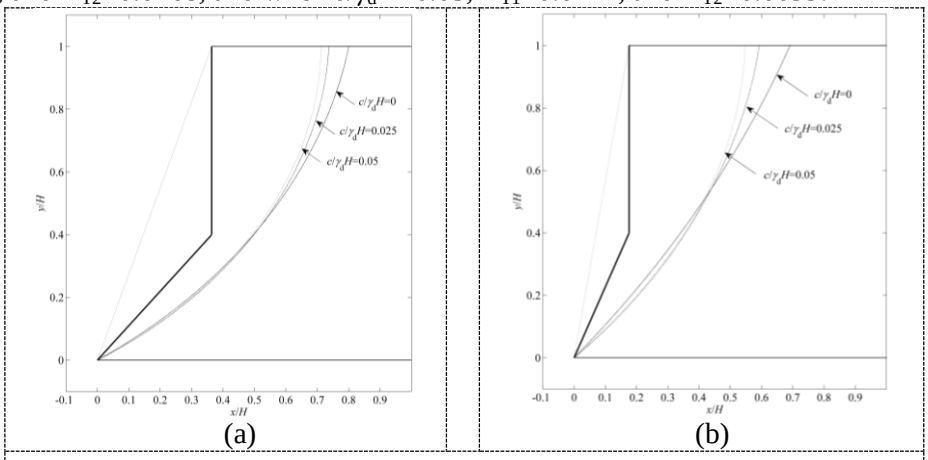

Figure 4. Critical slip surface under different c for λ=0.6: (*a*) α=70 °, and (*b*) α=80 °.

In Figure 5, traces of critical slip surfaces are presented for different values of Z_c while λ is equal to 0.6, α is equal to 70 °, $c/\gamma_d H$ is 0.025, and ϕ_d is equal to 34 °. With the increase of the value of Z_c/H, the critical slip surface moves towards the facing in the upper while moves away from the facing in the lower. When Z_c/H=0, K_{T1}=0.0253, and K_{T2}=0.0084. When Z_c/H=0.025, K_{T1}=0.0236, and K_{T2}=0.0083. When Z_c/H=0.05, K_{T1}=0.0218, and K_{T2}=0.0082.

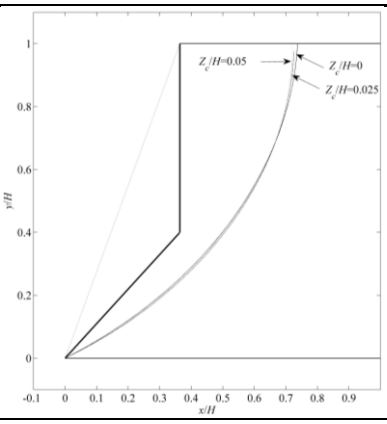

Figure 5. Critical slip surface under different Z_c for α=70 °and λ=0.6.

4. Conclusion

In the view of the fact that a cohesive material may be used as a reinforced fill, the LE approach using a top-down log spiral mechanism is presented to determine the internal stability analysis of the bilinear geosynthetic-reinforced slope in this paper. The formulation is then described, which it will result in the resultant reinforcement force required for the internal design of the bilinear geosynthetic-reinforced slope in the upper and lower tiers, respectively.

From stability charts, it is seen that the resultant reinforcement force in the upper tier increases as the ratio of the height of the upper tier to the height of the slope increases for different values of the cohesion while the resultant reinforcement force in the lower tier decreases in the same case. In addition, from critical slip surfaces, with the increase of the value of cohesion or depth of crack, the critical slip surface moves towards the facing in the upper while moves away from the facing in the lower, and the resultant reinforcement force in whether the upper or lower tier decreases. In a word, the presence of cohesion can produce design redundancy.

Acknowledgments

This study was sponsored by the Natural Science Foundation of Anhui Province (Grant No. 1608085QE121), the Fundamental Research Funds for the Central Universities (Grant No. JZ2015HGBZ0458), and the China Postdoctoral Science Foundation (Grant No. 2016M592048).

References

[1] Ruan, X., Leshchinsky, D., and Leshchinsky, B.A. 2015. Global stability of bilinear reinforced slopes. Transportation Infrastructure Geotechnology, 2(1), 34-46.
[2] Ruan, X., Guo, X., Luo, Y.-S., and Sun, S. 2017. Seismic design of bilinear geosynthetic-reinforced slopes. Soil Dynamics and Earthquake Engineering, 100, 454-457.
[3] Yang, G., Liu, H., Lv, P., and Zhang, B. 2012. Geogrid-reinforced lime-treated cohesive soil retaining wall: Case study and implications. Geotextiles and Geomembranes, 35, 112-118.
[4] Vahedifard, F., Leshchinsky, B.A., Sehat, S., Leshchinsky, D. 2014. Impact of cohesion on seismic design of geosynthetic-reinforced earth structures. Journal of Geotechnical and Geoenvironmental Engineering, 140(6), 04014016.
[5] Federal Highway Association (FHWA). 2009. Design and construction of mechanically stabilized earth walls and reinforced soil slopes, FHWA-NHI-10-024, Berg, R.R., Christopher, B.R., Samtani, N.C., eds. Washington, DC.